*J Mater Sci* (2017) 52:6754–6766

# Photocatalytic performance of $Cu_2O$-loaded $TiO_2$/rGO nanoheterojunctions obtained by UV reduction

Kaituo Dong[1,*], Jiandong He[1], Junxue Liu[2,3], Fengting Li[1], Lianqing Yu[1,*], Yaping Zhang[1], Xiaoyan Zhou[1], and Hongzhang Ma[1]

[1] College of Science, China University of Petroleum, Qingdao 266580, China
[2] College of Chemical Engineering, China University of Petroleum, Qingdao 266580, China
[3] State Key Laboratory of Molecular Reaction Dynamics, Dalian Institute of Chemical Physics, Chinese Academy of Sciences, 457 Zhong Shan Rd., Dalian 116023, China

**Received:** 7 September 2016
**Accepted:** 11 February 2017
**Published online:** 21 February 2017



## ABSTRACT

A novel dot-like $Cu_2O$-loaded $TiO_2$/reduced graphene oxide (rGO) nanoheterojunction was synthesized via UV light reduction for the first time. $Cu_2O$ with size of ca. 5 nm was deposited on rGO sheet and $TiO_2$ nanosheets. The products were characterized by infrared spectroscopy, Raman spectrum, UV–Vis diffuse reflectance spectra, XPS techniques, photoluminescence spectra. The results demonstrated that $Cu_2O$ and rGO enhanced the absorption for solar light, separation efficiency of electron–hole pairs, charge shuttle and transfer, and eventually improved photoelectrochemical and photocatalytic performance for contaminants degradation. The reaction time and anion precursor could affect the final copper-containing phase. As extending UV irradiation time, $Cu^{2+}$ was be first reduced to $Cu_2O$ and then transformed to metal Cu. In comparison with $CH_3COO^-$ (copper acetate), $NO_3^-$ (copper nitrate) and $Cl^-$ (copper chloride), $SO_4^{2-}$ (copper sulfate) was the optimum for synthesizing pure $Cu_2O$ phase.

## Introduction

Exploration of an optimum semiconductor nanoheterojunction architecture for enhanced photoelectrochemical properties had been developed with great efforts for years [1–5]. Varied architectures, such as bulk crystal/bulk crystal, core/shell, bulk crystal/dotted crystal et al., had been intensively studied [3, 6, 7]. Architecture of bulk crystal/dotted crystal was similar with a component of dye-sensitized or semiconductor quantum dot-sensitized $TiO_2$ in solar cell, owning high photoelectrochemical performance [8, 9]. For this architecture, dotted crystal with special structure and size had a tunable contact area on the surface of matrix [4, 10, 11]. $TiO_2$ nanosheets exposing (001) facet, which had excellent photocatalytic performance, made itself a stable substrate for building $TiO_2$-based heterojunctions architecture, while its wide band gap of 3–3.2 eV limited

Address correspondence to E-mail: dkt3030@163.com; iyy2000@163.com


DOI 10.1007/s10853-017-0911-2

the absorption of sun light. Loading dot-like semiconductor with response of visible light on $TiO_2$ nanosheets might be an optimum architecture.

Cuprous oxide ($Cu_2O$) was a relative stable p-type semiconductor with direct band gap of 2.0–2.2 eV which could absorb visible light below 600 nm [12, 13]. In addition, its conduction and valence band positions matched well with those of n-type $TiO_2$, which facilitated separation of photo-induced electron–hole pairs [13–15]. However, $TiO_2$ nanosheet/dot-like $Cu_2O$ crystal heterojunction still had poor electron conductivity [16]. Reduced graphene oxide (rGO) owning graphitic $sp^2$ and $sp^3$-hybrid structures had comparable conductivity of metal and large surface area as a substrate for building heterojunctions [17, 18]. It is reported that particles of $TiO_2$ or $Cu_2O$ combining with rGO had enhanced charge shuttle and transfer performance [13, 19, 20]. So the dot-like $Cu_2O$-loaded $TiO_2$/rGO nanoheterojunction might become one of the most efficient $TiO_2$-based photocatalysts.

General method for loading dot-like $Cu_2O$ crystal on the $TiO_2$ or rGO is reduction of various cupric salts with strong chemical reagents in alkaline condition at high temperature [14, 21, 22]. For example, Wang or Geng et al. [14, 23] synthesized nanocrystalline $Cu_2O$ on $TiO_2$ frame or arrays using cupric acetate as precursor and glucose as reducing reagent. Gao et al. [24] loaded $Cu_2O$ particle on rGO sheet using L-ascorbic acid as reductive reagent in mild condition. Compared to chemical liquid reduction, photochemical synthesis of $Cu_2O$ had advantages of free chemical reagents addition, room temperature, atmospheric pressure, free of pH adjustment via alkali or acid. In previous reports, $Cu_2O$ was synthesized via γ-ray radiation [25, 26]. However, γ-ray radiated by $^{60}Co$ source is very environmental unfriendly, harmful and strictly restricted by laws.

In this work, γ-ray was alternated by a ultraviolent (UV) light (main peak 254 nm, 25 W), and dot-like $Cu_2O$ crystal with size of ca. 5 nm was successfully deposited on $TiO_2$ nanosheet/rGO. To our knowledge, this has never been reported before. The results revealed that the newly designed nanoheterojunction had strong absorption of solar light, high separation efficiency of electron–hole pairs and high performance of charge shuttle and transfer. Surfactants such as sodium dodecyl benzene sulfonate (SDBS) existing in cleaning agents, dyes such as methyl orange (MO), rhodamine B (RhB) as the aromatic-containing macromolecules existing in waste water were selected to evaluate its photocatalytic activity [27].

More importantly, various cupric salts with different anions such as $SO_4^{2-}$, $Cl^-$, $CH_3COO^-$, $NO_3^-$ were employed to synthesize $Cu_2O$ in previous works [14, 28–30]. In this report, taken different stabilities, chemical activities and chelating ability with positive ion into consideration, these cupric salts as precursors were studied to explore the synthetic mechanism under photochemical condition.

## Experiment

### Materials

Natural graphite was purchased from Qingdao Baichun graphitic Co., Ltd. Fluorine tin oxide (FTO)-coated glass (resistivity <10 Ω $sq^{-1}$) was purchased from Zhuhai Kaivo Electronic Components Co., Ltd. The other chemical reagents were purchased from Sinopharm chemical reagent Co., Ltd. And all the chemicals were used without further purification.

### Synthesis of graphite oxide

Graphite oxide was synthesized by the typical modified Hummers' method [31]. In details, 2 g of natural graphite flakes was mixed with 1 g sodium nitrate in the ice bath. Then, 50 mL concentrated $H_2SO_4$ was slowly added into the mixture under stirring to keep temperature under 5 °C. 0.3 g potassium permanganate was slowly put into the mixture under stirring to maintain temperature below 20 °C. Then, 7 g potassium permanganate was slowly added into the mixture for 1 h to keep temperature below 20 °C. Successively, the mixed solution was stirred at 35 °C for 2 h, followed by slow addition of deionized (DI) water (90 mL). After that, the solution was heated to 98 °C and kept for 15 min. The suspension was further diluted with 55 mL DI warm water, and then, 7 mL $H_2O_2$ was added to terminate the reaction. The mixture was filtered and washed with 10% HCl (1 L) and DI water (1 L) until pH 7. The graphite oxide product was vacuum-dried at 40 °C for 12 h.

### Synthesis of $TiO_2$ nanosheets

The $TiO_2$ nanosheets were synthesized by hydrothermal method [32]. In a typical experimental procedure, 5 mL of tetrabutyl titanate [$Ti(OBu)_4$,

≥98%] and 0.6 mL of hydrofluoric acid (HF) (≥40%) were mixed in a dried Teflon autoclave with a capacity of 20 mL, and kept at 180 °C for 24 h. The powder was separated by centrifugation, washed by water and ethanol several times, consecutively. The final product was vacuum-dried at 80 °C for 6 h. Caution! HF is extremely corrosive and a contact poison, and it should be handled with extreme care. Hydrofluoric acid solution should be stored in plastic container and used in a fume hood.

## Synthesis of $TiO_2/Cu_2O$ composite

20 mg $TiO_2$ nanosheets were sonicated in 100 mL ethanol for 15 min and then poured into 100 ml $CuSO_4$ aqueous solution (containing 3 mmol $CuSO_4{\cdot}5H_2O$) with fiercely stirring. The following procedure was the same with the $Cu_2O$ synthesis (shown in supporting information), and this obtained $TiO_2/Cu_2O$ composite was labeled as TC.

## Synthesis of $TiO_2/rGO/Cu_2O$ composites

10 mg graphite oxide was sonicated in 100 mL deionized water at 30–40 °C for 30 min to obtain clear suspension; then, 3 mmol $CuSO_4{\cdot}5H_2O$ was added and dissolved. The following synthesis procedure was as same as that of TC and labeled as TGC (6 h UV light irradiation).

Other samples with irradiation of 2, 4, 12 h (donated as TGC-2, TGC-4, TGC-12 h) are also prepared.

Several other cupric salts [such as $CuCl_2$, $Cu(CH_3COO)_2$, $Cu(NO_3)_2$] were employed to substitute $CuSO_4$ to obtain final products labeled as TGC-Cl2, TGC-A, TGC-N (6 h UV light irradiation).

## Photoelectrochemical performance

The photoelectrochemical measurement was performed by a CHI 760E electrochemical workstation (Shanghai CH instrument Co., Ltd, China), with Pt plate as counter electrode, Ag/AgCl (filled with 3.5 M KCl aqueous solution) as reference electrode and 0.2 M $Na_2SO_4$ aqueous solution as electrolyte. The working electrode was prepared as follows: 10 mg product powder was mixed with 22 μL PVDF poly(vinylidene fluoride) solution, and that PVDF was dissolved in *N*-methyl-2-pyrrolidone (wt% 5%) with weight ratio of 90:10 to make slurry. The film was made by doctor blade method on FTO for area of $1\times1$ $cm^2$, then vacuum-dried at 100 °C for 12 h. The uncovered area of FTO which would be immersed in electrolyte was protected by insulting glue.

## Photocatalytic performance

The photocatalytic performance was measured by photodegradation of MO, RhB and SDBS. In a typical process, 20 mg of photocatalysts and 100 mL MO/SDBS/RhB solution (20 mg $L^{-1}$) were sonicated for 10 min to obtain homogeneous suspension. Before light irradiation, the suspension was stirred for 0.5 h in dark to achieve adsorption and desorption equilibrium. Then, 5 mL of the solution was extracted every 0.5 h for UV–Vis absorption measurement. The photoreaction was carried out in the protection of cycling cool water. The light source is 350 W Xenon lamp to simulate solar light (range of spectrum is from 200 to 2500 nm).

## Characterization

Powder X-ray diffraction (XRD) was performed on DX-2700 X-ray diffractometer (Dandong Fangyuan, China) with monochromatized Cu-Kα radiation ($\lambda = 1.5418$ Å) at 40 kV and 30 mA. Transmission electron microscopy (TEM) images were taken with JEOL JEM-2100 transmission electron microscope at 200 kV. The concentration of MO was analyzed by measuring the light absorption at 484 nm UV–Vis 756PC Spectrophotometer (Shanghai Spectrum Instruments Co., Ltd. China). Fourier transform infrared (FTIR) spectra were obtained using BRUKER Tensor II spectrometer in the frequency range of 4000–400 $cm^{-1}$ with a resolution of 4 $cm^{-1}$. Measurement of Raman spectra was performed on a Raman DXR Microscope (Thermo Fisher, USA) with excitation laser beam wavelength of 532 nm. PL spectrum was measured at room temperature on a 7-PLSpec fluorescence spectrophotometer (Saifan, China). The wavelength of the excitation light is 325 nm. Optical absorption spectra were recorded on a UV–Vis spectrometer (UV-2600, Shimadzu, Japan) over a spectral range of 200–1400 nm. X-ray photoelectron spectroscopy (XPS, Thermo ESCALAB 250XI) with Al Kα ($hv = 1486.6$ eV) radiation and beam spot of 500 μm was operated at 150 W. The Brunauer–Emmett–Teller (BET) surface areas were characterized by a surface area analyzer

(Micromeritics, ASAP2020 M, USA) with nitrogen adsorption at 77 K.

## Results and discussion

### Characterization of phase and morphology

The XRD peaks of crystalline $Cu_2O$ were observed in Fig. S2a and 1 for TC and TGC, which indicated $Cu_2O$ (PDF#05-0667) could be synthesized under UV radiation directly without assistance of any chemical reagent at room temperature. Peaks of crystallized anatase $TiO_2$ (PDF#21-1272) were observed in the TC and TGC samples. Graphene oxide (GO) fabricated by Hummers' method in aqueous solution was reduced to rGO under the UV irradiation [31, 33, 34], which was also demonstrated by IR spectrum shown in Fig. 3a. However, no GO or rGO peak was found since ordered stacking of rGO sheets had been disrupted by loading $TiO_2$ nanosheets and $Cu_2O$ [33].

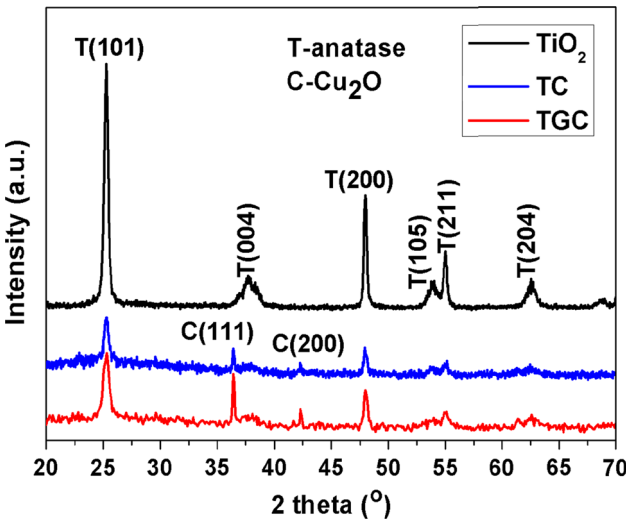


**Figure 1** XRD patterns of $TiO_2$, TC, TGC samples.

$TiO_2$ nanosheets were prepared by the classical hydrothermal method [32], which had rectangular shape with the length of ca. 50 nm and thickness of 5 nm, as shown in Fig. S1. As $Cu_2O$ composited with $TiO_2$ forming sample TC, large amounts of $Cu_2O$ nanocrystals were deposited on $TiO_2$ nanosheets and even self-aggregated because of large quantities, as shown in Fig. 2a. After further compositing with rGO, it is observed that large amounts of $Cu_2O$ nanocrystal with size of ca. 5 nm adhered on $TiO_2$ nanosheets and rGO sheet in Fig. 2b, c, which was ascribed to residual oxygen-containing groups of rGO facilitating dispersion of $Cu^+$. This new morphology was achieved only via UV irradiation without addition of any chemical reducing reagent, so this work provides a novel way for synthesizing nano-$Cu_2O$ and its composites.

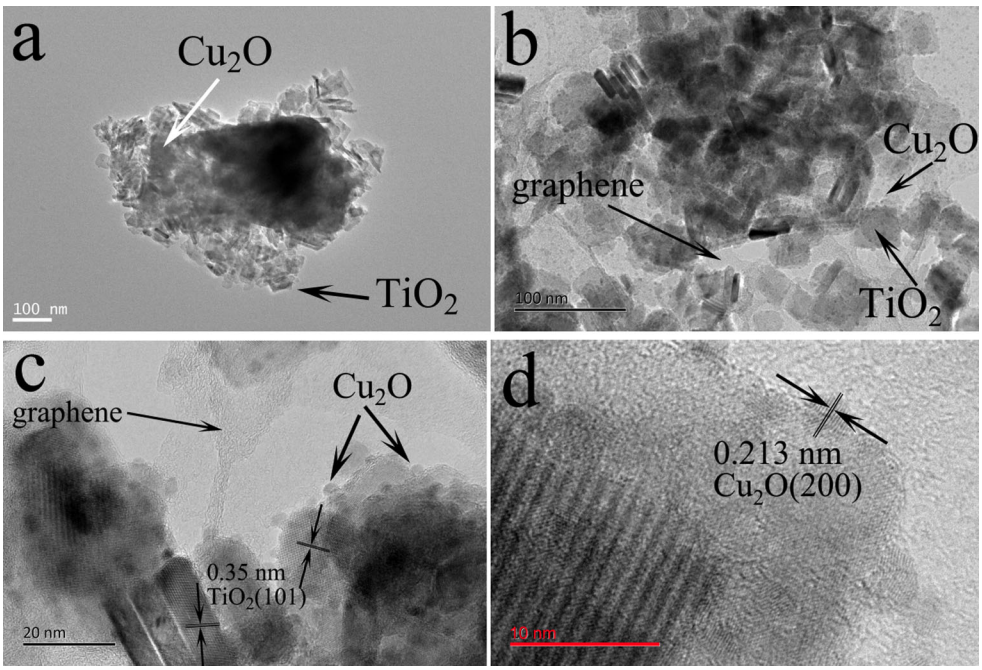


**Figure 2** TEM of sample TC (**a**), TGC (**b**, **c**); HRTEM of $Cu_2O$ nanocrystals (**d**), displaying the (200) exposed facet, with lattice space of 0.213 nm.

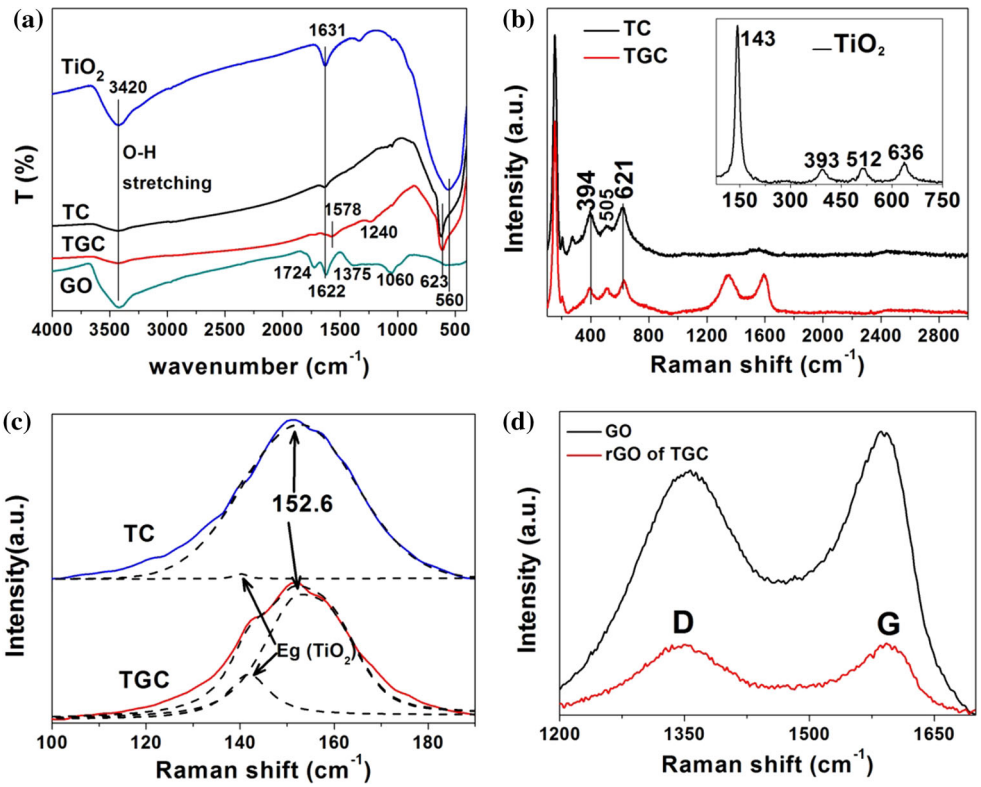


**Figure 3** **a** FTIR spectrum of $TiO_2$, TC, TGC, GO samples; **b** Raman spectrum of TC and TGC samples, the *inset* is anatase $TiO_2$; **c** Fitting of Raman bands of TC and TGC by Lorentzian–Gaussian functions; **d** Raman spectra of rGO in TGC and GO.

## Characterization of IR and Raman spectrum

Chemical bond and phases of composites were characterized by FRIT and Raman spectrum (Fig. 3). In Fig. 3a, around 3420 $cm^{-1}$ corresponded to the O–H stretching vibration of alcoholic or phenolic groups as well as intercalated or adsorbed water molecular for all samples [35–38]. The peak of 1631 $cm^{-1}$ was attributed to bending mode of surface –OH or water for $TiO_2$, TC [39]. The broadband around 560 $cm^{-1}$ between 880 and 400 $cm^{-1}$ showed the vibration of Ti–O–Ti bonds of sample $TiO_2$, TC, TGC [40]. The sharp peak of 623 $cm^{-1}$ was attributed to the stretching of copper(I)–O bond in TC and TGC, which indicated the formation of $Cu_2O$ [41]. In comparison with stretching modes of carbonyl (C=O) bond (1724 $cm^{-1}$), conjugation absorption for bending mode of water and C=C $sp^2$ hybrid(1622 $cm^{-1}$), tertiary alcohol (C–OH) bending (1375) and alkoxy (C–O) vibrations (1060) in IR spectrum of GO, most oxygen-containing groups of rGO in TGC were removed by the UV reduction [42, 43], its absorption peak of C=C bond was shifted to 1578 $cm^{-1}$. The 1240 $cm^{-1}$ peak should be attributed to stretching modes of the epoxy (C–O–C) group that can hardly removed by UV irradiation [44].

In Fig. 3b, four strong vibration peaks at 143 $cm^{-1}$ ($E_g$), 393 $cm^{-1}$ ($B_{1g}$), 512 $cm^{-1}$ ($A_{1g}$) and 615 $cm^{-1}$ ($E_{1g}$) were ascribed to the five Raman active modes ($A_{1g} + B_{1g} + 3E_g$) of anatase [45]. The peaks around 120–180 $cm^{-1}$ for TC and TGC were decomposed to the sharp peak at 152.6 $cm^{-1}$, which should be mainly attributed to the $\Gamma_{15}^{(1)}$ (LO) infrared (ir)-allowed mode in perfect $Cu_2O$ crystals and a small peak for $E_g$ mode of anatase as shown in Fig. 3c [46]. The peak at 505 and 621 $cm^{-1}$ should be assigned to the overlapping of Raman vibration mode of crystalline $Cu_2O$ and $TiO_2$ [45, 47]. The peak at 394 $cm^{-1}$ was the $B_{1g}$ mode of anatase $TiO_2$ for TC and TGC. Phase determination of Raman spectra agreed with the results of XRD (Fig. 1). D band provided information about defect of graphitic structure and the presence of $sp^3$-hybridized domain [17]. G band was a prominent feature of the pristine graphite, corresponding to the first-order scattering of the $E_{2g}$ mode [48]. In Fig. 3d, the position of D and G band of GO was about 1357 and 1586 $cm^{-1}$, respectively. After reduction, the D and G band for rGO of TGC shifted to 1350, 1592 $cm^{-1}$, respectively, and $I_D/I_G$ increased from 0.91 to 1.13 after UV reduction of GO, which indicated a decrease in average size and increase in

numbers of the $sp^2$-hybridized domains of rGO in TGC, comparing with that of GO [48, 49].

## XPS analysis

Figure 4a demonstrates the full spectrum of sample TGC, while Fig. 4b–d focuses on the specific binding energy of element Ti, Cu and C, respectively. The Ti 2*p* peaks located at the binding energies of 459.0 and 464.8 eV were attributed to Ti $2p_{3/2}$ and Ti $2p_{1/2}$, which corresponded to $Ti^{4+}$ [50]. In Fig. 4c, the peak for Cu $2p_{3/2}$ was decomposed into two peaks, the main peak of which at 932.6 eV was the characteristic of $Cu^{+}$ in $Cu_2O$ [28], and the peak at 934.1 eV indicated the existence of $Cu^{2+}$ in CuO [51]. XPS could only detect the shallow surface elements composition, so the observation of $Cu^{2+}$ indicated the oxidation of a small portion of $Cu_2O$ during sample drying and handing under normal ambient condition. This phenomenon had been reported by many researchers on the synthesis of $Cu_2O$ nanoparticles. From C 1*s* XPS spectrum of GO (Fig. 4d), the peaks at 282.8, 286.7, 288.5 eV were assigned to the $sp^2$-hybrid bond (C–C, C=C, C–H), C–O and O–C=O bond, respectively [52]. After UV reduction, a large amount of C–O and O–C=C bonds were removed as indicated by the decrease in intensities of these two peaks, which was consistent with results of IR spectra.

## Selective adsorption and photocatalytic performance

Photocatalytic performances of samples were characterized by degradation of MO, SDBS and RhB (Fig. 5a–c). All experiments were carried out in nearly neutral solution, shown in Table S1. The MO is no self-degradation. Pure $TiO_2$ nanosheets had the lowest degradation ability for 26.7%, while sample TC had stronger degradation ability (50.9%) after compositing with $Cu_2O$. Further incorporation of rGO can facilitate MO adsorption, and thus, the TGC had highest photocatalytic activity for MO degradation (70.6%). For SDBS degradation, $TiO_2$ had lowest photocatalytic activity (20.8%). Sample TGC had slightly better activity than TC (ca. 70%). For RhB degradation, $TiO_2$ still had poorest activity than others because of its absorbance limitation of solar light. TC had better photocatalytic performance than TGC. As shown in Fig. 5d, within 2.5 h, MO and SDBS could be decomposed dramatically by TC and TGC under solar light; however, the degradation efficiency for RhB was much lower than that for other

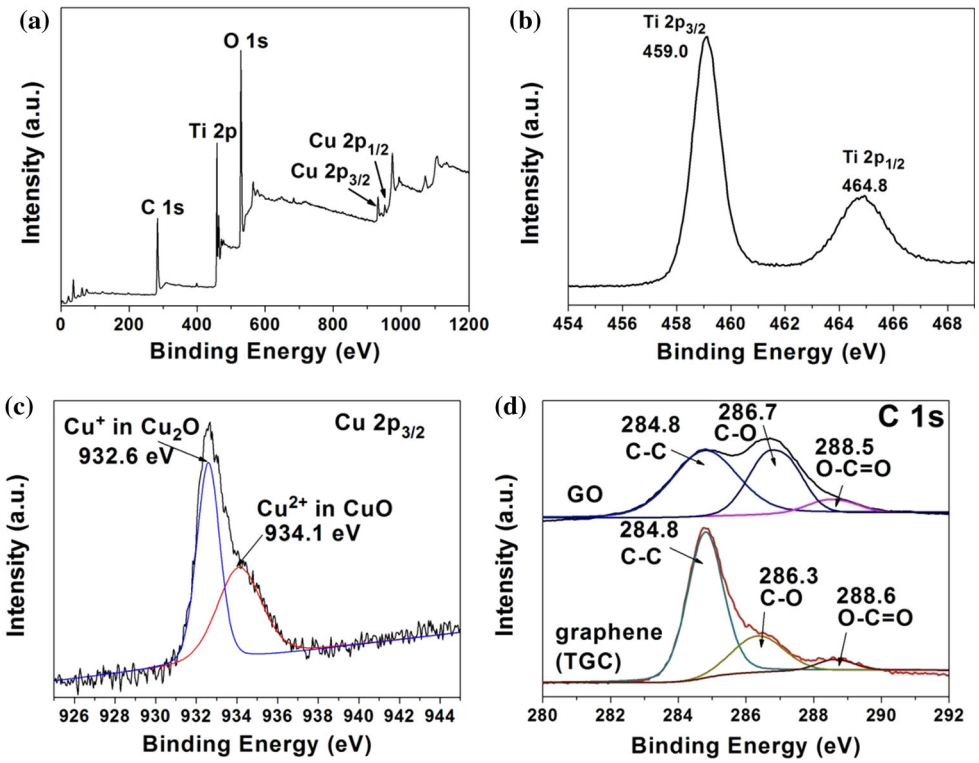


**Figure 4** XPS spectra of TGC sample calibrated at C 1 s 284.8 eV, **a** full spectrum, **b** Ti 2p spectrum, **c** Cu $2p_{3/2}$ spectrum and **d** C 1 s for TGC and GO spectra.

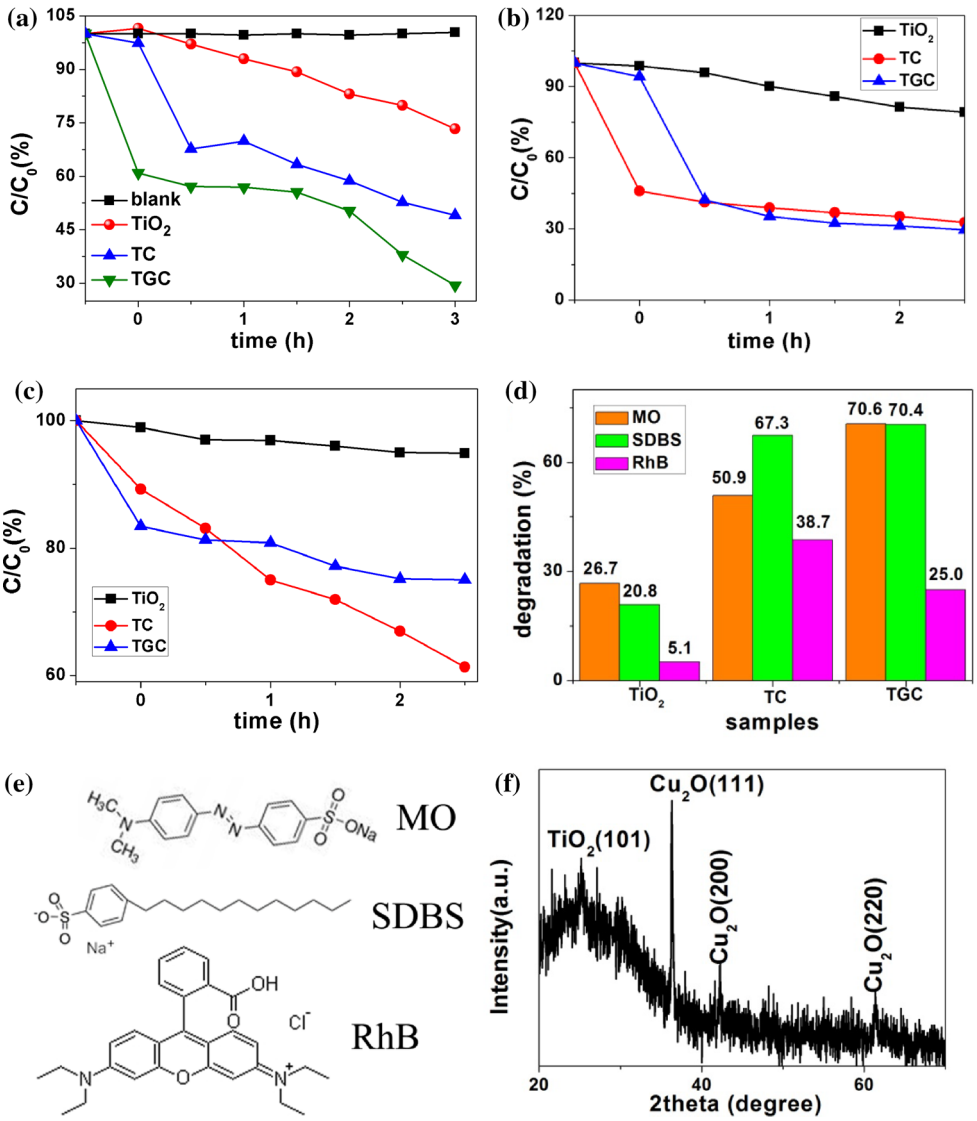


**Figure 5** Photocatalytic degradation performance of **a** MO, **b** SDBS and **c** RhB, under irradiation of 350 W Xenon lamp simulating solar light AM1.5; **d** comparison of photodegradation for MO, SDBS and RhB; **e** molecule structure of MO, SDBS and RhB; **f** XRD pattern of TGC after 12 h under simulated solar light.

contaminations, which indicated that only some special contaminations could be decomposed by nanoheterojunction effectively.

The adsorption of photocatalysts for contaminations played an important role in the process of photocatalytic reactions. Contaminants owning opposite charge with the photocatalysts could easily adsorb on the surface of photocatalysts preferentially. However, given that the charge of MO/SDBS/RhB (molecule structures are shown in Fig. 5e) in aqueous solution and adsorption abilities of the synthesized photocatalysts, the reverse charge principle was not perfect for explaining adsorption difference. Taken some special groups of contaminants into consideration, nitrogen-containing groups may also affect the eventual adsorption outcome.

Chemical stability of $Cu_2O$ particles is one of predominant factors for photochemical applications. Exposed to UV light (irradiated by varied lamp), $Cu_2O$ can be reduced to metal Cu [53, 54]. However, in this work under standard simulated solar light, $Cu_2O$ was very stable and no metal copper was found even after 12 h with the characterization of X-ray diffraction (Fig. 5f).

## Photocatalytic mechanism

As shown in Fig. 6a, $TiO_2$ could only absorb UV light below 387 nm. $Cu_2O$ enhanced absorption of visible light below 640 nm in TC. Moreover, with incorporation of rGO, TGC had highest light absorbance, so it induced more photo-induced charge carriers and

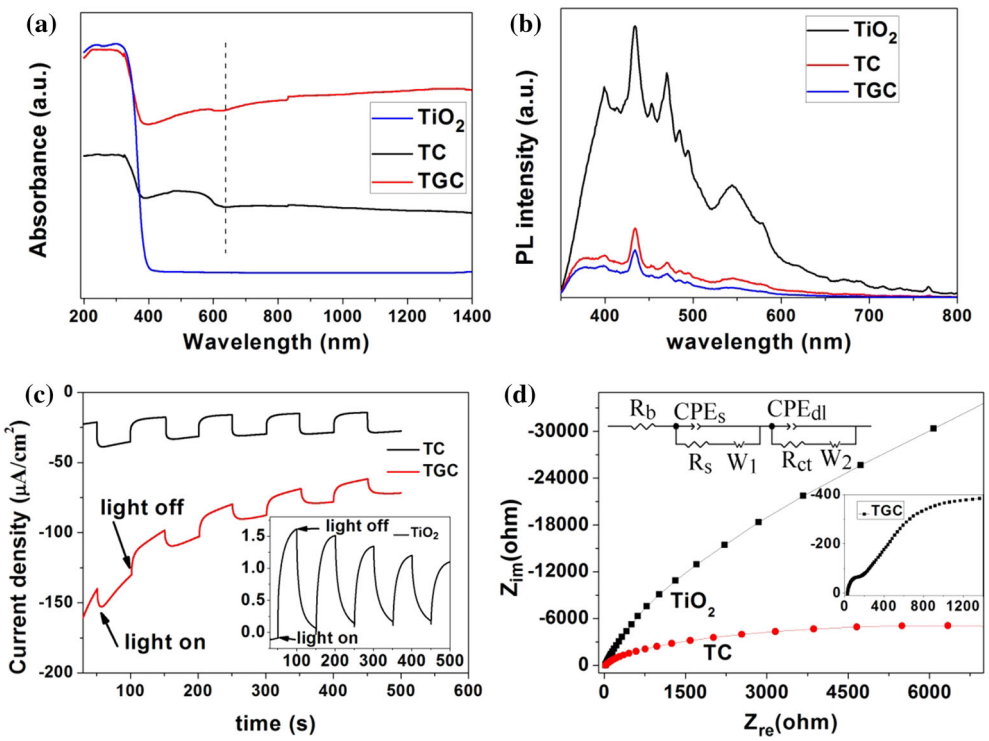


**Figure 6** **a** UV–Vis diffuse reflectance spectra of $TiO_2$, TC, TGC; **b** PL spectrum of $TiO_2$, TC, TGC; **c** photocurrent curve of $TiO_2$ (*inset*), TC and TGC under simulated solar light; **d** electrochemical impedance spectrum (EIS) of $TiO_2$, TC and TGC (*inset*).

higher degradation rate. Optical band gap of composite was calculated using Tauc plot shown in Fig. S3d [55]. Comparing with pure $TiO_2$ (3.2 eV), optical band gap of TC and TGC decreased to 2.72 and 2.64 eV, respectively.

PL spectrum was employed to characterize separation efficiency of photo-generated electron–hole pairs. As shown in Fig. 6b, several peaks such as 400, 434, 470, 544 nm were observed in PL spectrum of $TiO_2$, which attributed to electron transition from the conduction band to valence band, band-edge free excitons, oxygen vacancies or surface defect [56, 57]. TC had lower intensity of PL than pure $TiO_2$ that inferred $Cu_2O$ could accept the photocharge from $TiO_2$. Furthermore, lowest intensity of TGC demonstrated that rGO could further accept the photo-induced electron and enhance separation efficiency of electron–hole pairs.

$TiO_2$ electrode in $Na_2SO_4$ aqueous solution had a positive photocurrent, indicating its n-type semiconductor nature, shown in inset of Fig. 6c. Oppositely, sample TC and TGC exhibited a negative current response and larger photocurrent, which was a sign of p-type semiconductor of $Cu_2O$ (also demonstrated in Fig. S2b). In addition, $Cu_2O$ could also enhance the charge transportation in TC, compared to the current baseline of $TiO_2$. The rGO further enhanced the conductivity of TGC. As shown in Fig. 6d, the typical electrochemical impedance spectra were presented as Nyquist plots. For fitting the EIS, equivalent circuit [model: R(Q(RW))(Q(RW))] was demonstrated that the simulating results fitted the experimental very well. Q is constant phase element (CPE). $R_b$ represented the bulk resistance, CPEs should be considered in the nonhomogeneous condition of the composites, associating with the capacitor, and $R_s$ are the resistance of the solid-state interface layer which is formed at the highly charged state due to the passivation reaction between the electrolyte and the surface of the electrode, corresponding to the first semicircle at high frequency [58]. $CPE_{dl}$ and $R_{ct}$ are the double-layer capacitance and the charge-transfer resistance, corresponding to the second semicircle at medium frequency. Nyquist plots of EIS showed that nanocrystalline $Cu_2O$ could decrease the $R_{ct}$ from $9.4\times10^5$ to $1.2\times10^4$ ohm $cm^2$ for TC because of the smaller semicircle at the medium frequency, in comparison with $TiO_2$ (Fig. 6d) [40]. The resistance of TGC dramatically decreased to 4.4 ohm $cm^2$ because of high conductivity of rGO as shown in inset of

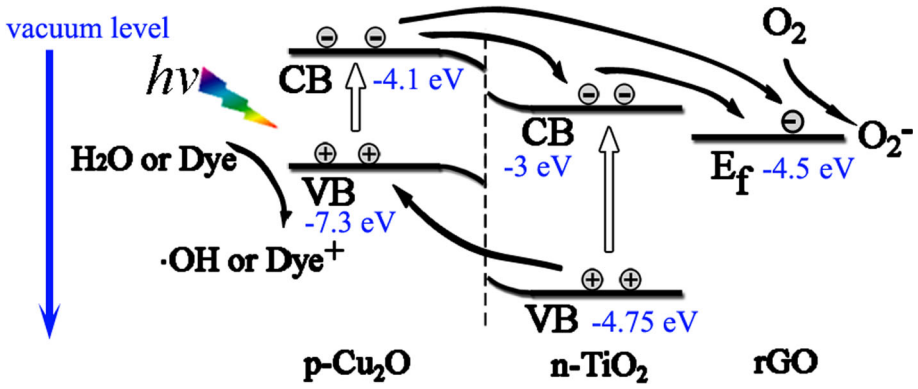


**Figure 7** Illustration of transfer of photo-generated electron–hole pairs excited by solar light. The dissolved $O_2$ scavenge the photo-generated electron transferred from $Cu_2O$ or $TiO_2$ to form $O_2^-$, the photohole oxidized $H_2O$ to OH or decompose dye directly. Band gaps of $TiO_2$ and $Cu_2O$ were determined by UV–Vis diffuse reflection spectroscopy. Energy levels referred to Refs. 22, 59–61.

Fig. 6d. Its high charge shuttle and transfer enhanced the degradation ability.

Photocatalytic performance of TGC was the best in the photocatalysts for MO and SDBS degradation. The schematic illustration is shown in Fig. 7: (1) The band gap of $Cu_2O$ determined by UV–Vis diffuse reflection spectroscopy (Fig. S3b) is 1.75 eV, which could enhance visible light absorption below 708 nm, generating more electron–hole pairs; (2) the matching energy band structure facilitated the separation of electron–hole pairs of heterojunction [15, 29, 62]; (3) rGO facilitated the dispersion of nanocrystals, transfer and shuttle of photo-generated electron in metal oxide particles [63].

## Reduction mechanism of TGC via UV

Figure 8a shows the effect of irradiation time on phase of products. No $Cu_2O$ could be detected by the XRD after 2-h reaction. If the reaction prolonged for 4 h, a weak peak (111) of $Cu_2O$ could be observed, then more $Cu_2O$ were synthesized after 6 h. However, when the UV reduction time extended to 12 h, part of $Cu_2O$ particle converted to metal Cu.

Several other cupric salts [such as $CuCl_2$, $Cu(CH_3COO)_2$, $Cu(NO_3)_2$] were tried to synthesize $Cu_2O$ products, labeled as TGC-Cl2, TGC-A, TGC-N (other synthesizing conditions were the same as that of sample TGC). There was $CH_3COOCu$ (PDF#28-0392) formed under UV reduction with $(CH_3COO)^-$ involvement, shown in Fig. 8b. As $NO_3^-$ used, the final phases of TGC-N could not be identified at present. As $Cl^-$ used, all XRD peaks for TGC-Cl2 were assigned to anatase and no copper-containing phase was detected. Furthermore, if NaCl was added to the TGC synthesis process, no diffraction peaks of copper-containing phase were found either (shown in Fig. 8b donated as TGC-Cl). It demonstrated that $Cl^-$ could chelate $Cu^+$ preferentially instead of $OH^-$.

Above all, the mechanism of synthesizing $Cu_2O$ could be proposed as follows:

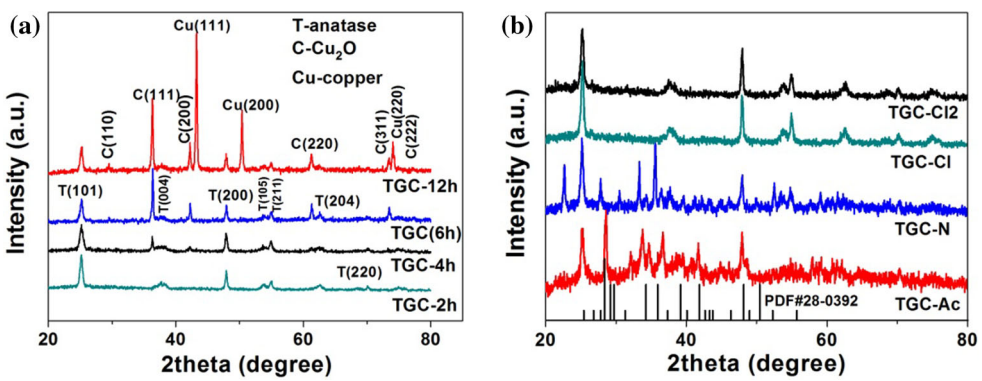


**Figure 8** XRD patterns of **a** TGC-2 h, TGC-4 h, TGC (6 h), TGC-12 h and **b** TGC-A, TGC-N, TGC-Cl2, TGC-Cl.

$$H_2O \xrightarrow{h\nu} H^+ + H\cdot + \cdot OH + e^-_{aq} \ldots etc$$
$$\cdot OH + CH_3CH_2OH \rightarrow CH_3\dot{C}OH + H_2O$$
$$Cu^{2+} + e^-_{aq} \rightarrow Cu^+$$
$$Cu^+ + OH^- \rightarrow CuOH$$
$$2CuOH \rightarrow Cu_2O + H_2O$$

If extending irradiation time, there would be:

$$Cu_2O + 2e^- + H_2O \rightarrow 2Cu + 2OH^-$$

If CH3COO$^-$ was employed as the precursor:

$$Cu^{2+} + e^-_{aq} \rightarrow Cu^+$$
$$Cu^+ + OH^- + CH_3COO^- \rightarrow CH_3COOCu + OH^-$$

If $Cl^-$ was added into the reaction system of TGC, the reaction was changed to:

$$Cu^{2+} + e^-_{aq} \rightarrow Cu^+$$
$$Cu^+ + OH^- + Cl^- \rightarrow CuCl_{aq} + OH^-$$

So compared to $CH_3COO^-/NO_3^-/Cl^-$, $SO_4^{2-}$ is the optimum anion for UV reduction synthesis of $Cu_2O$.

## Conclusion

Pure $Cu_2O$, $TiO_2/Cu_2O$, $TiO_2/rGO/Cu_2O$ nanoheterojunctions were fabricated by novel UV reduction method, and large amounts of dot-like $Cu_2O$ nanocrystals with size of ca. 5 nm were formed on the rGO or $TiO_2$ nanosheets. Sample TGC achieved the strongest absorption for solar light, highest separation efficiency of photo-induced electron–hole pairs. It had p-type photocurrent response under solar light and excellent photocatalytic performance. The adsorption abilities for catalysts varied with different dyes or surfactant, determined by nitrogen-containing groups and surface charge. Extending irradiation time could convert $Cu_2O$ to metal copper. In comparison with $CH_3COO^-/NO_3^-/Cl^-$, $SO_4^{2-}$ is the optimum anion for synthesis of pure $Cu_2O$ phase under UV condition.

## Acknowledgements

The financial support for this study by National Natural Science Foundation of China (No. 21476262), the Technology Development Plan of Qingdao (No. 14-2-4-108-jch) and Research Funds for the Central Universities (15CX05032A, 15CX05056A) is gratefully acknowledged.



**Electronic supplementary material:** The online version of this article (doi:10.1007/s10853-017-0911-2) contains supplementary material, which is available to authorized users.

## References

[1] Wang H, Zhang L, Chen Z, Hu J, Li S, Wang Z, Liu J, Wang X (2014) Semiconductor heterojunction photocatalysts: design, construction, and photocatalytic performances. Chem Soc Rev 43(15):5234–5244. doi:10.1039/c4cs00126e

[2] Bessegato G, Guaraldo T, de Brito J, Brugnera M, Zanoni M (2015) Achievements and trends in photoelectrocatalysis: from environmental to energy applications. Electrocatalysis 6(5):415–441. doi:10.1007/s12678-015-0259-9

[3] Rajeshwar K, de Tacconi NR, Chenthamarakshan CR (2001) Semiconductor-based composite materials: preparation, properties, and performance. Chem Mater 13(9):2765–2782. doi:10.1021/cm010254z

[4] Chen H, Li W, Liu H, Zhu L (2011) Performance enhancement of CdS-sensitized $TiO_2$ mesoporous electrode with two different sizes of CdS nanoparticles. Microporous Mesoporous Mater 138(1–3):235–238. doi:10.1016/j.micromeso.2010.09.021

[5] Yu L, Zhang Y, Zhi Q, Wang Q, Gittleson FS, Li J, Taylor AD (2015) Enhanced photoelectrochemical and sensing performance of novel $TiO_2$ arrays to $H_2O_2$. Sens Actuator B: Chem 211:111–115. doi:10.1016/j.snb.2015.01.060

[6] Tamiolakis I, Lykakis IN, Armatas GS (2015) Mesoporous CdS-sensitized $TiO_2$ nanoparticle assemblies with enhanced photocatalytic properties: selective aerobic oxidation of benzyl alcohols. Catal Today 250:180–186. doi:10.1016/j.cattod.2014.03.047

[7] Banin U, Ben-Shahar Y, Vinokurov K (2014) Hybrid semiconductor-metal nanoparticles: from architecture to function. Chem Mater 26(1):97–110. doi:10.1021/cm402131n

[8] Chen H, Fu W, Yang H, Sun P, Zhang Y, Wang L, Zhao W, Zhou X, Zhao H, Jing Q, Qi X, Li Y (2010) Photosensitization of $TiO_2$ nanorods with CdS quantum dots for

photovoltaic devices. Electrochim Acta 56(2):919–924. doi:10.1016/j.electacta.2010.10.003

[9] O'Regan B, Gratzel M (1991) A low-cost, high-efficiency solar cell based on dye-sensitized colloidal $TiO_2$ films. Nature 353(6346):737–740

[10] Lin Z-Q, Lai Y-K, Hu R-G, Li J, Du R-G, Lin C-J (2010) A highly efficient ZnS/CdS@$TiO_2$ photoelectrode for photogenerated cathodic protection of metals. Electrochim Acta 55(28):8717–8723. doi:10.1016/j.electacta.2010.08.017

[11] Wang C, Jiang Z, Wei L, Chen Y, Jiao J, Eastman M, Liu H (2012) Photosensitization of $TiO_2$ nanorods with CdS quantum dots for photovoltaic applications: a wet-chemical approach. Nano Energy 1(3):440–447. doi:10.1016/j.nanoen.2012.02.005

[12] Hara M, Kondo T, Komoda M, Ikeda S, Kondo JN, Domen K, Shinohara K, Tanaka A (1998) $Cu_2O$ as a photocatalyst for overall water splitting under visible light irradiation. Chem Commun 3:357–358. doi:10.1039/a707440i

[13] Tran PD, Wong LH, Barber J, Loo JSC (2012) Recent advances in hybrid photocatalysts for solar fuel production. Energy Environ Sci 5(3):5902–5918. doi:10.1039/c2ee02849b

[14] Wang M, Sun L, Lin Z, Cai J, Xie K, Lin C (2013) p-n heterojunction photoelectrodes composed of $Cu_2O$-loaded $TiO_2$ nanotube arrays with enhanced photoelectrochemical and photoelectrocatalytic activities. Energy Environ Sci 6(4):1211–1220. doi:10.1039/c3ee24162a

[15] Ola O, Maroto-Valer MM (2015) Review of material design and reactor engineering on $TiO_2$ photocatalysis for $CO_2$ reduction. J Photochem Photobiol C 24:16–42. doi:10.1016/j.jphotochemrev.2015.06.001

[16] Pelaez M, Nolan NT, Pillai SC, Seery MK, Falaras P, Kontos AG, Dunlop PSM, Hamilton JWJ, Byrne JA, O'Shea K, Entezari MH, Dionysiou DD (2012) A review on the visible light active titanium dioxide photocatalysts for environmental applications. Appl Catal B 125:331–349. doi:10.1016/j.apcatb.2012.05.036

[17] Pei S, Cheng H-M (2012) The reduction of graphene oxide. Carbon 50(9):3210–3228. doi:10.1016/j.carbon.2011.11.010

[18] Fernández-Merino MJ, Guardia L, Paredes JI, Villar-Rodil S, Solís-Fernández P, Martínez-Alonso A, Tascón JMD (2010) Vitamin C is an ideal substitute for hydrazine in the reduction of graphene oxide suspensions. J Phys Chem C 114(14):6426–6432. doi:10.1021/jp100603h

[19] Bell NJ, Ng YH, Du A, Coster H, Smith SC, Amal R (2011) Understanding the enhancement in photoelectrochemical properties of photocatalytically prepared $TiO_2$-reduced graphene oxide composite. J Phys Chem C 115(13):6004–6009. doi:10.1021/jp1113575

[20] Yu L, Dong K, Zhang Y, Wang Q, Zhi Q (2014) Tuned n/n or n/p heterojunctions for reduced graphene oxide and titania nanosheets and their electrochemical properties. Mater Chem Phys 148(3):803–809. doi:10.1016/j.matchemphys.2014.08.052

[21] Talebian A, Entezari MH, Ghows N (2013) Complete mineralization of surfactant from aqueous solution by a novel sono-synthesized nanocomposite ($TiO_2$–$Cu_2O$) under sunlight irradiation. Chem Eng J 229:304–312. doi:10.1016/j.cej.2013.05.117

[22] Zhang S, Peng B, Yang S, Fang Y, Peng F (2013) The influence of the electrodeposition potential on the morphology of $Cu_2O/TiO_2$ nanotube arrays and their visible-light-driven photocatalytic activity for hydrogen evolution. Int J Hydrogen Energy 38(32):13866–13871. doi:10.1016/j.ijhydene.2013.08.081

[23] Geng Z, Zhang Y, Yuan X, Huo M, Zhao Y, Lu Y, Qiu Y (2015) Incorporation of $Cu_2O$ nanocrystals into $TiO_2$ photonic crystal for enhanced UV–Visible light driven photocatalysis. J Alloy Compd 644:734–741. doi:10.1016/j.jallcom.2015.05.075

[24] Gao Z, Liu J, Xu F, Wu D, Wu Z, Jiang K (2012) One-pot synthesis of graphene–cuprous oxide composite with enhanced photocatalytic activity. Solid State Sci 14(2):276–280. doi:10.1016/j.solidstatesciences.2011.11.032

[25] Miao W, Liu H, Zhang Z, Chen J (2008) Large-scale growth and shape evolution of micrometer-sized $Cu_2O$ cubes with concave planes via γ-irradiation. Solid State Sci 10(10):1322–1326. doi:10.1016/j.solidstatesciences.2008.01.015

[26] Liu H, Miao W, Yang S, Zhang Z, Chen J (2009) Controlled synthesis of different shapes of $Cu_2O$ via γ-irradiation. Cryst Growth Des 9(4):1733–1740. doi:10.1021/cg800703n

[27] Fujishima A, Zhang X, Tryk DA (2008) $TiO_2$ photocatalysis and related surface phenomena. Surf Sci Rep 63(12):515–582. doi:10.1016/j.surfrep.2008.10.001

[28] Liu L, Yang W, Li Q, Gao S, Shang JK (2014) Synthesis of $Cu_2O$ nanospheres decorated with $TiO_2$ nanoislands, their enhanced photoactivity and stability under visible light illumination, and their post-illumination catalytic memory. ACS Appl Mater Interfaces 6(8):5629–5639. doi:10.1021/am500131b

[29] Praveen Kumar D, Lakshmana Reddy N, Mamatha Kumari M, Srinivas B, Durga Kumari V, Sreedhar B, Roddatis V, Bondarchuk O, Karthik M, Neppolian B, Shankar MV (2015) $Cu_2O$-sensitized $TiO_2$ nanorods with nanocavities for highly efficient photocatalytic hydrogen production under solar irradiation. Sol Energy Mater Sol Cells 136:157–166. doi:10.1016/j.solmat.2015.01.009

[30] Zhang J, Liu W, Wang X, Wang X, Hu B, Liu H (2013) Enhanced decoloration activity by $Cu_2O$@$TiO_2$ nanobelts heterostructures via a strong adsorption-weak photodegradation process. Appl Surf Sci 282:84–91. doi:10.1016/j.apsusc.2013.05.054

[31] Hummers WS, Offeman RE (1958) Preparation of graphitic oxide. J Am Chem Soc 80(6):1339. doi:10.1021/ja01539a017

[32] Han X, Kuang Q, Jin M, Xie Z, Zheng L (2009) Synthesis of titania nanosheets with a high percentage of exposed (001) facets and related photocatalytic properties. J Am Chem Soc 131(9):3152–3153. doi:10.1021/ja8092373

[33] Tu Y, Ichii T, Utsunomiya T, Sugimura H (2015) Vacuum-ultraviolet photoreduction of graphene oxide: electrical conductivity of entirely reduced single sheets and reduced micro line patterns. Appl Phys Lett 106(13):133105. doi:10.1063/1.4916813

[34] Zhang Y-L, Guo L, Xia H, Chen Q-D, Feng J, Sun H-B (2014) Photoreduction of graphene oxides: methods, properties, and applications. Adv Opt Mater 2(1):10–28. doi:10.1002/adom.201300317

[35] Dong K, Yu L, Zhang Y, Wang Q, Neppolian B (2014) Green synthesis of sulfur/graphene nanocomposite and photocatalytic performance. Sci Adv Mater 6(8):1828–1835. doi:10.1166/sam.2014.1948

[36] Mathkar A, Tozier D, Cox P, Ong P, Galande C, Balakrishnan K, Leela Mohana Reddy A, Ajayan PM (2012) Controlled, stepwise reduction and band gap manipulation of graphene oxide. J Phys Chem Lett 3(8):986–991. doi:10.1021/jz300096t

[37] Nethravathi C, Rajamathi M (2008) Chemically modified graphene sheets produced by the solvothermal reduction of colloidal dispersions of graphite oxide. Carbon 46(14):1994–1998. doi:10.1016/j.carbon.2008.08.013

[38] Kim UJ, Furtado CA, Liu X, Chen G, Eklund PC (2005) Raman and IR Spectroscopy of chemically processed single-walled carbon nanotubes. J Am Chem Soc 127(44):15437–15445. doi:10.1021/ja052951o

[39] Li G, Li L, Boerio-Goates J, Woodfield BF (2005) High purity anatase $TiO_2$ nanocrystals: near room-temperature synthesis, grain growth kinetics, and surface hydration chemistry. J Am Chem Soc 127(24):8659–8666. doi:10.1021/ja050517g

[40] Zhang H, Lv X, Li Y, Wang Y, Li J (2010) P25-graphene composite as a high performance photocatalyst. ACS Nano 4(1):380–386. doi:10.1021/nn901221k

[41] Hou C, Quan H, Duan Y, Zhang Q, Wang H, Li Y (2013) Facile synthesis of water-dispersible $Cu_2O$ nanocrystal-reduced graphene oxide hybrid as a promising cancer therapeutic agent. Nanoscale 5(3):1227–1232. doi:10.1039/c2nr32938g

[42] Collins WR, Schmois E, Swager TM (2011) Graphene oxide as an electrophile for carbon nucleophiles. Chem Commun 47(31):8790–8792. doi:10.1039/c1cc12829a

[43] Colthup N (2012) Introduction to infrared and Raman spectroscopy. Elsevier, Amsterdam

[44] Si Y, Samulski ET (2008) Synthesis of water soluble graphene. Nano Lett 8(6):1679–1682. doi:10.1021/nl080604h

[45] Wang Y, Y-n Zhang, Zhao G, Tian H, Shi H, Zhou T (2012) Design of a novel $Cu_2O/TiO_2$/carbon aerogel electrode and its efficient electrosorption-assisted visible light photocatalytic degradation of 2,4,6-Trichlorophenol. ACS Appl Mater Interfaces 4(8):3965–3972. doi:10.1021/am300795w

[46] Powell D, Compaan A, Macdonald JR, Forman RA (1975) Raman-scattering study of ion-implantation-produced damage in $Cu_2O$. Phys Rev B 12(1):20–25

[47] Wu L, L-k Tsui, Swami N, Zangari G (2010) Photoelectrochemical stability of electrodeposited $Cu_2O$ films. J Phys Chem C 114(26):11551–11556. doi:10.1021/jp103437y

[48] Tuinstra F, Koenig JL (1970) Raman spectrum of graphite. J Chem Phys 53(3):1126–1130. doi:10.1063/1.1674108

[49] Stankovich S, Dikin DA, Piner RD, Kohlhaas KA, Kleinhammes A, Jia Y, Wu Y, Nguyen ST, Ruoff RS (2007) Synthesis of graphene-based nanosheets via chemical reduction of exfoliated graphite oxide. Carbon 45(7):1558–1565. doi:10.1016/j.carbon.2007.02.034

[50] Fang WQ, Zhou JZ, Liu J, Chen ZG, Yang C, Sun CH, Qian GR, Zou J, Qiao SZ, Yang HG (2011) Hierarchical structures of single-crystalline anatase $TiO_2$ nanosheets dominated by 001 facets. Chem A Eur J 17(5):1423–1427. doi:10.1002/chem.201002582

[51] Yin M, Wu C-K, Lou Y, Burda C, Koberstein JT, Zhu Y, O'Brien S (2005) Copper oxide nanocrystals. J Am Chem Soc 127(26):9506–9511. doi:10.1021/ja050006u

[52] Wang W-S, Wang D-H, Qu W-G, Lu L-Q, Xu A-W (2012) Large ultrathin anatase $TiO_2$ nanosheets with exposed 001 facets on graphene for enhanced visible light photocatalytic activity. J Phys Chem C 116(37):19893–19901. doi:10.1021/jp306498b

[53] Lalitha K, Sadanandam G, Kumari VD, Subrahmanyam M, Sreedhar B, Hebalkar NY (2010) Highly stabilized and finely dispersed $Cu_2O/TiO_2$: a promising visible sensitive photocatalyst for continuous production of hydrogen from glycerol: water mixtures. J Phys Chem C 114(50):22181–22189. doi:10.1021/jp107405u

[54] Xu S, Sun DD (2009) Significant improvement of photocatalytic hydrogen generation rate over $TiO_2$ with deposited CuO. Int J Hydrogen Energy 34(15):6096–6104. doi:10.1016/j.ijhydene.2009.05.119

[55] Li Y, Wang B, Liu S, Duan X, Hu Z (2015) Synthesis and characterization of $Cu_2O/TiO_2$ photocatalysts for $H_2$

evolution from aqueous solution with different scavengers. Appl Surf Sci 324:736–744. doi:10.1016/j.apsusc.2014.11.027

[56] Liu B, Wang X, Cai G, Wen L, Song Y, Zhao X (2009) Low temperature fabrication of V-doped $TiO_2$ nanoparticles, structure and photocatalytic studies. J Hazard Mater 169(1–3):1112–1118. doi:10.1016/j.jhazmat.2009.04.068

[57] Liqiang J, Honggang F, Baiqi W, Dejun W, Baifu X, Shudan L, Jiazhong S (2006) Effects of Sn dopant on the photoinduced charge property and photocatalytic activity of $TiO_2$ nanoparticles. Appl Catal B 62(3–4):282–291. doi:10.1016/j.apcatb.2005.08.012

[58] He B-L, Dong B, Li H-L (2007) Preparation and electrochemical properties of Ag-modified $TiO_2$ nanotube anode material for lithium–ion battery. Electrochem Commun 9(3):425–430. doi:10.1016/j.elecom.2006.10.008

[59] Jung HS, Park N-G (2015) Perovskite solar cells: from materials to devices. Small 11(1):10–25. doi:10.1002/smll.201402767

[60] Huang L, Peng F, Ohuchi FS (2009) "In situ" XPS study of band structures at $Cu_2O/TiO_2$ heterojunctions interface. Surf Sci 603(17):2825–2834. doi:10.1016/j.susc.2009.07.030

[61] Giovannetti G, Khomyakov PA, Brocks G, Karpan VM, van den Brink J, Kelly PJ (2008) Doping graphene with metal contacts. Phys Rev Lett 101(2):026803

[62] Liu L, Gu X, Sun C, Li H, Deng Y, Gao F, Dong L (2012) In situ loading of ultra-small $Cu_2O$ particles on $TiO_2$ nanosheets to enhance the visible-light photoactivity. Nanoscale 4(20):6351–6359. doi:10.1039/c2nr31859h

[63] Wang X, Zhi L, Müllen K (2008) Transparent, conductive graphene electrodes for dye-sensitized solar cells. Nano Lett 8(1):323–327. doi:10.1021/nl072838r